Electronic Supplementary Material (ESI) for Dalton Transactions.

Supporting Information

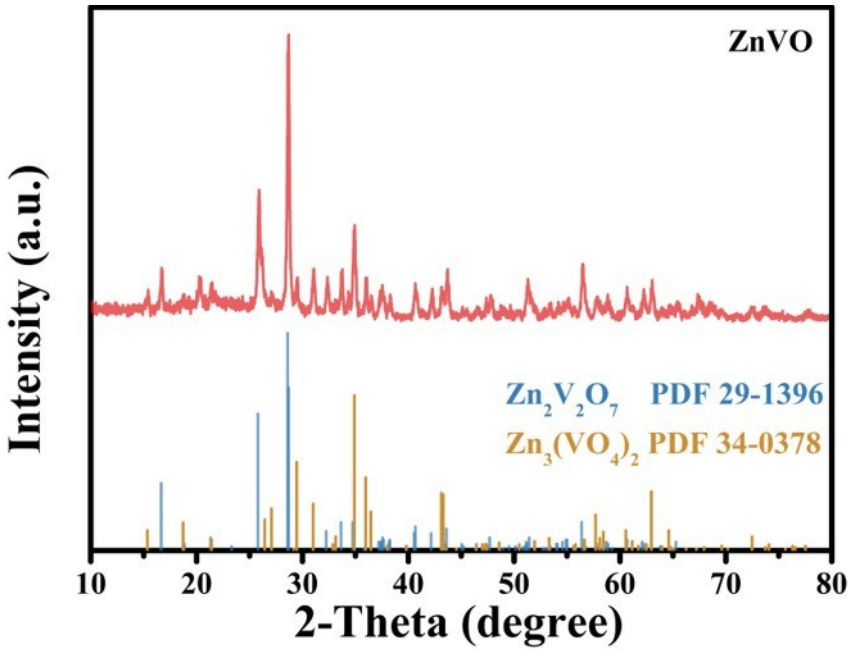

Fig. S1. XRD patterns of ZnVO after heating in air for Zn-V-OH.

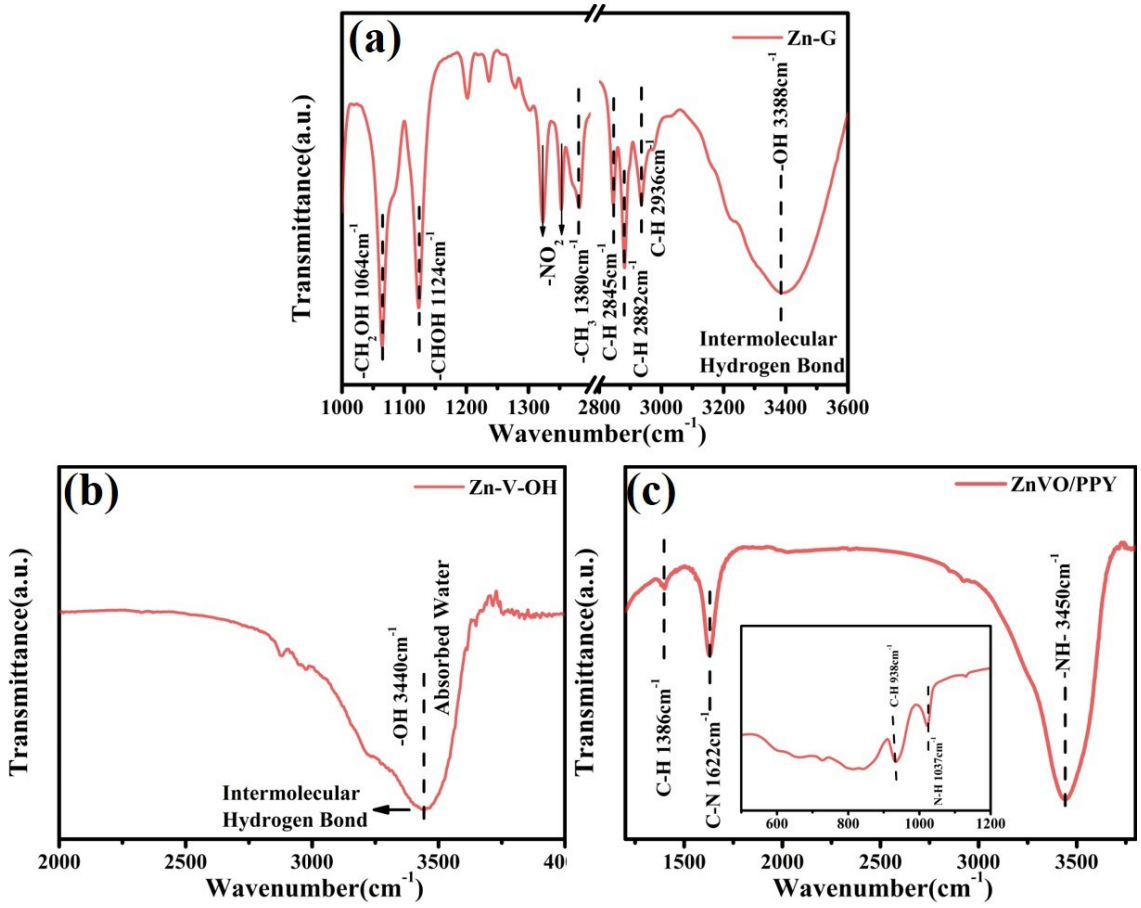

Fig. S2. FTIR spectrum of (a) the Zn-G microspheres, (b) Zn-V-OH and (c) ZnVO/PPY composite.

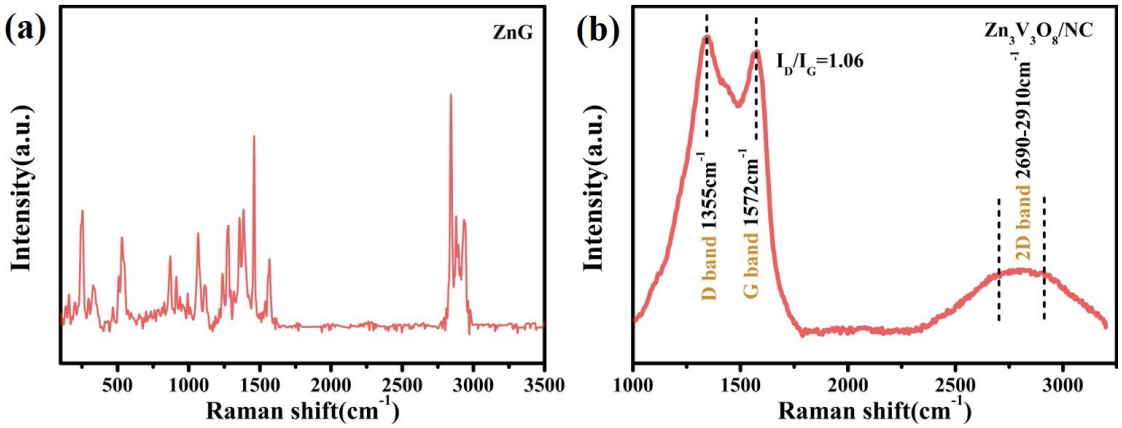

Fig. S3 Raman spectra of (a) Zn-G microspheres and (b) $Zn_3V_3O_8$/NC composite.

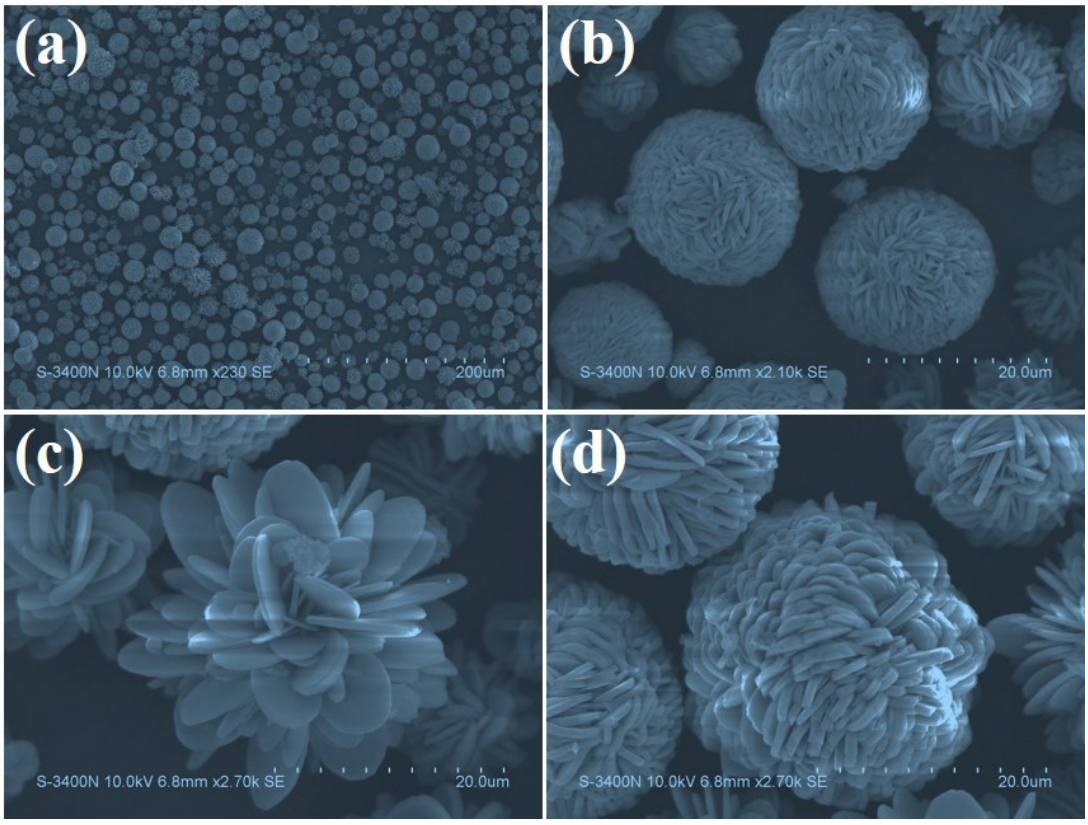

Fig. S4. FESEM images of the Zn-V-OH microspheres.

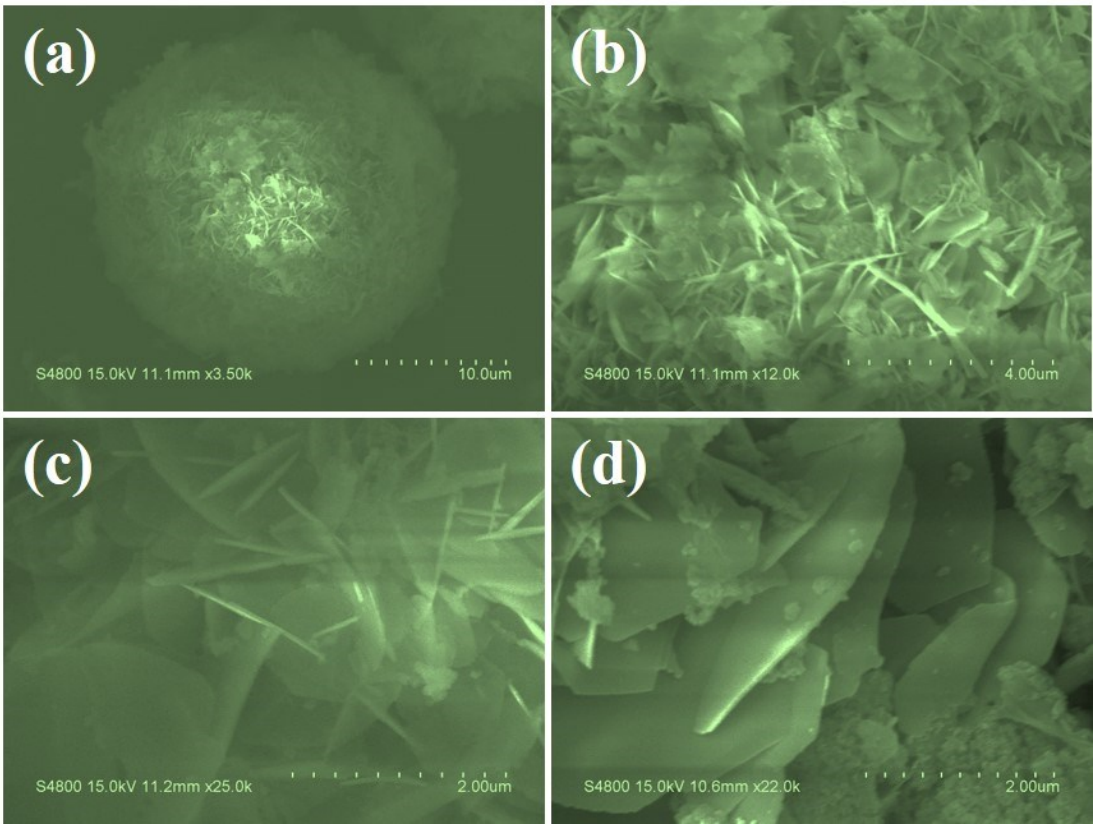

Fig. S5. FESEM images of ZnVO/PPY composite microspheres.

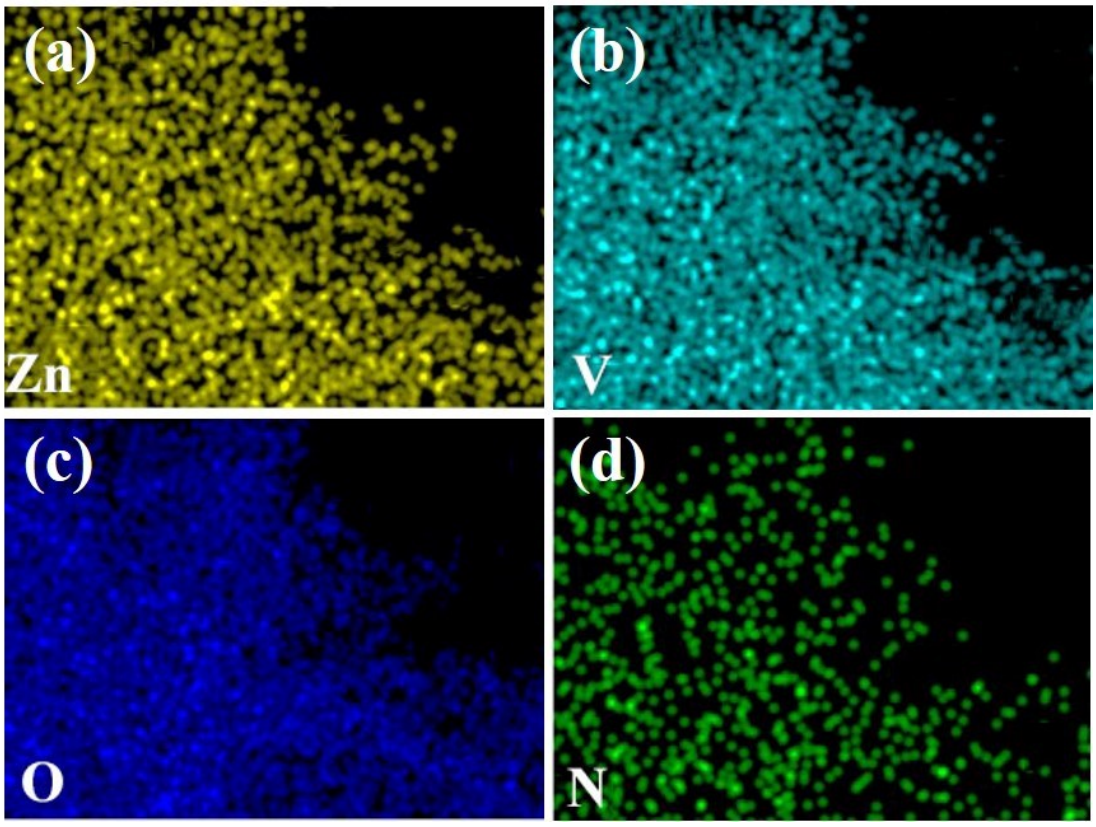

Fig. S6. EDS mappings of Zn, V, O and N for a nanosheet of $Zn_3V_3O_8$/NC composite.

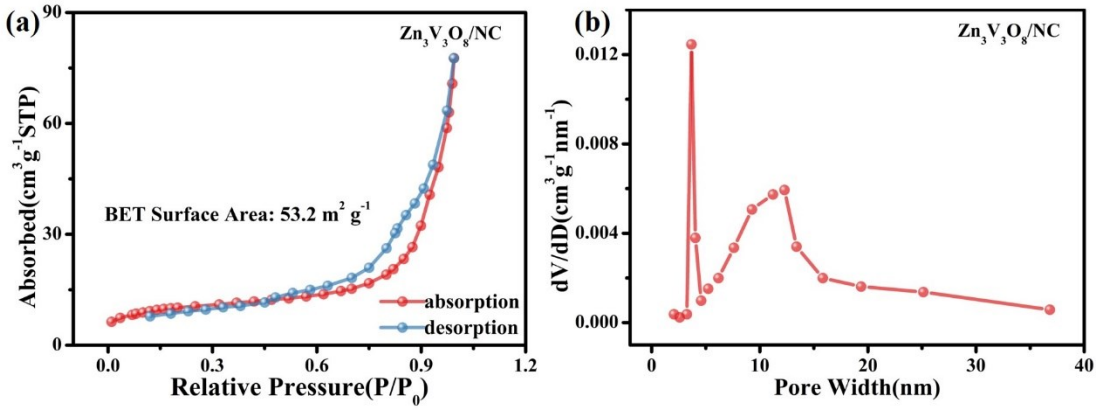

Fig. S7. (a) Nitrogen adsorption/desorption isotherms and (b) pore size distribution of $Zn_3V_3O_8$/NC composite.

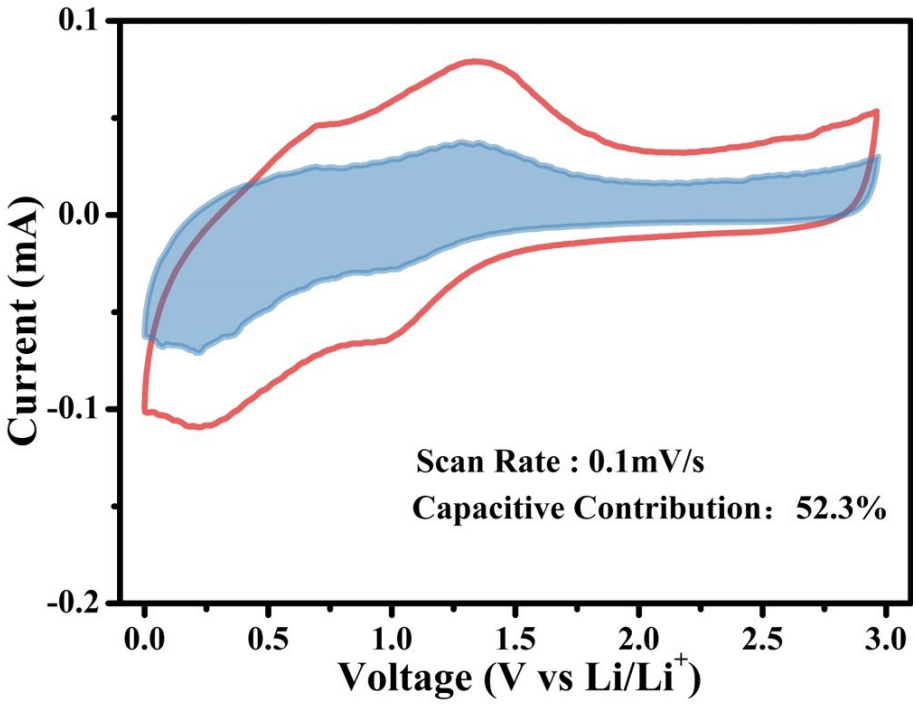

Fig. S8. Capacitive contribution at the scan rate of 0.1 mV/s for $Zn_3V_3O_8$/NC composite as anode for lithium ion batteries.

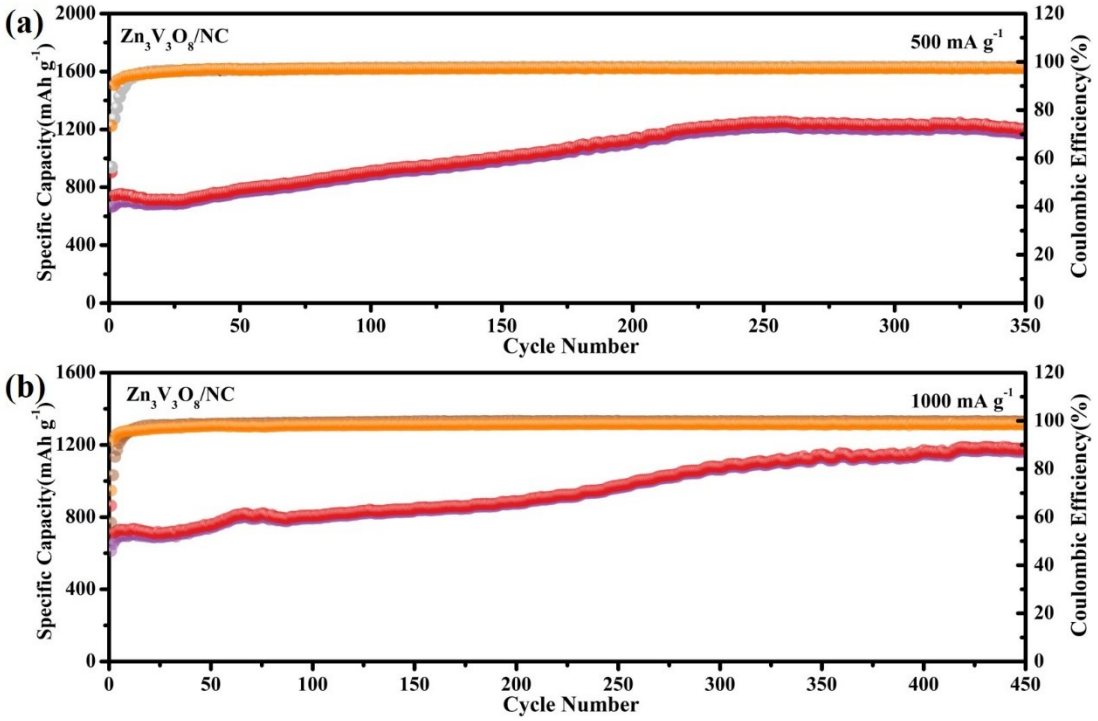

Fig. S9. Cycling performance and coulombic efficiency of $Zn_3V_3O_8$/NC composite as anode for lithium ion batteries at the current densities of (a) 500 mA g^{-1} and (b) 1000 mA g^{-1}.

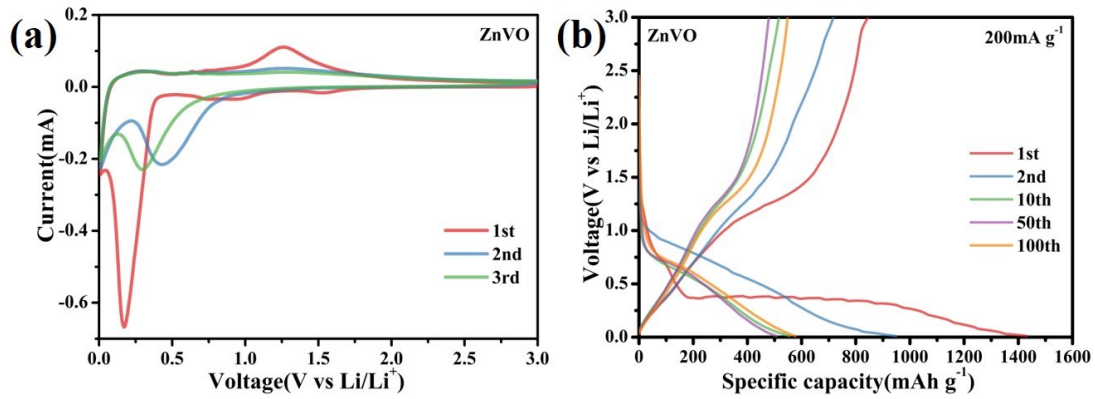

Fig. S10. Electrochemical performances of ZnVO composite as anode for lithium ion batteries. (a) The initial three cyclic voltammetry at a scan rate of 0.1 mV s^{-1}. (b) The 1^{st}, 2^{nd}, 10^{th}, 50^{th} and 100^{th} galvanostatic discharge/charge curves within a voltage window of 0.01-3.0 V at a current density of 200 mA g^{-1}.

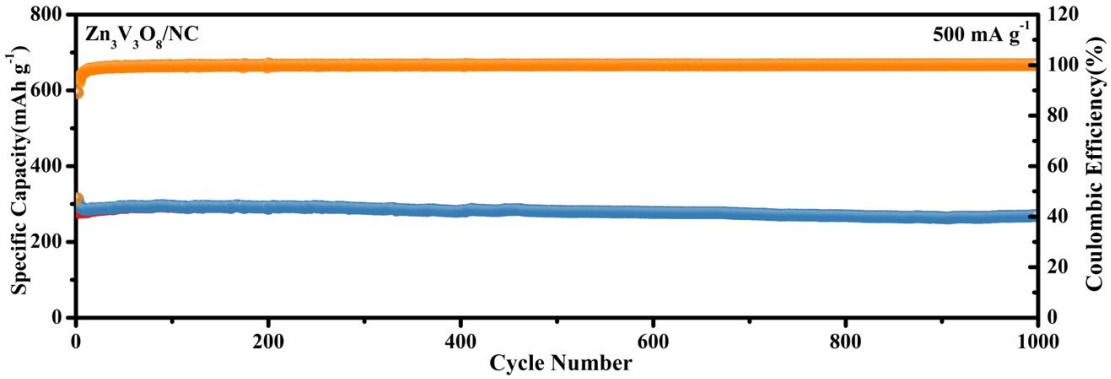

Fig. S11. Cycling stability at 500 mA g^{-1} for $Zn_3V_3O_8$/NC composite as anode for sodium ion batteries.